Available at www.sciencedirect.com

ScienceDirect

journal homepage: www.elsevier.com/locate/he

Nanoscale carbon material porosity effect on gas adsorption

S. Beyaz[a], F. Darkrim Lamari[b,*], B. Weinberger[b], P. Langlois[b]

[a] University of Kocaeli, Umuttepe Yerleskesi, Faculty Arts and Science, Chem. Department 41380 Izmit, Turkey
[b] LIMHP Université Paris 13 CNRS UPR1311; Institut Galilée, 99 Av. J.B.Clément, 93430 Villetaneuse, France

ARTICLE INFO

ABSTRACT

In this paper, we discussed the potential of hydrogen adsorption by three types of carbon materials (GNF, SWNT and AC) in relation with their surface reactivity due to their nanometric pore dimension. We realized experimental studies of hydrogen adsorption measurements on a high accuracy gravimetric device up to 5 MPa on a series of chemically activated carbons and nanomaterials offering a wide range of porosities. Comparison with a very high pressure volumetric device up to 70 MPa is also given. We used in the mass balance, the material skeleton density determined at 700 K. Samples were characterized by Raman spectroscopy, XRD, TEM and BET methods. Material analysis correlation with macroscopic gas adsorption helps to the phenomenon interpretation at molecular scale. Although gas-solid interactions are weak; the adsorption sites are dense and their accessibility is an important point for optimizing gas uptake by increasing material porosity development. We discuss the limitations of the physical adsorption as a storage tool.

© 2009 Professor T. Nejat Veziroglu. Published by Elsevier Ltd. All rights reserved.

1. Introduction

Carbon nanomaterials have attracted the attention of many scientists because of their potential applications in the development of hydrogen-fueled vehicles. The carbon-based materials have been considered as potential storage materials in view of their low cost, easy accessibility, low densities, interesting recycling characteristics, various bulk and pore structures, material chemical stability, possibility to synthesize diverse carbon structures and possibility to activate their surface by post-synthesis processes. In the last years, promising experimental results claiming high hydrogen adsorption capacities of carbon materials have been reported in the literature (cf. Tables 1 and 2). Two mechanisms could explain hydrogen adsorption in porous carbon materials: i) adsorption on the surface of the porous carbon ii) adsorption in the internal space of the porous carbon. In both cases, the specific

surface area and the pore volume of the materials play an important role. The Tables 1 and 2 group the results of hydrogen gravimetric storage capacities in weight percent wt.% reported by different authors in the last years for porous carbon adsorbents. Contrarily to simulation results which clearly demonstrate that the optimization of hydrogen adsorption excess can lead to a storage up to 2 wt.% at room temperature and high pressure and to 6 wt% at 77 K [1–3], experimental results are much dispersed in the literature. High hydrogen concentrations in carbon nanotubes reported in the literature [4] have induced the publication of an important number of studies using carbon materials like single walled carbon nanotubes (SWNT) and graphite nanofiber (GNF) prepared by arc discharge, laser vaporization, High Pressure CO dissociation process (HiPco) and Chemical Vapor Deposition (CVD) methods. In parallel, simulation results have been reported early in order to interpret the results in relation

---

Table 1 – Hydrogen storage capacities in SWNT at different conditions collected from literature. The purity rate and the method of purification are noted in the 1st column. 2nd column gives the diameter of the materials when available; the 3rd column gives the specific surface area of the materials in $m^2 g^{-1}$. The measurement method is given in the 4th column. The 5th column shows the degassing conditions (temperature: K, pressure: MPa, time: hour); the 6th column represents the measurement conditions and the 7th column represents the hydrogen adsorption capacity of the materials in weight percent (wt.%).

Nanotubes	D (nm)	SBET (m²/g)	Set up	Degassing conditions	T(K), P(MPa)	wt.%	References
Laser (raw)	1.2	–	TPD	–	300, 0.065	0.01	[4]
Arc (raw, 40%)	1.1–1.4	250	G	873 K	84, 1	0.68	[19]
Arc (purified)	–	95	G	873 K	84, 1	0.45	[19]
HiPco (purified)	–	–	V	673 K	298,7	0.43	[21]
Arc (raw)	1.2	350	V	673 K	293, 6	0.2	[22]
Arc (350 °C air/1 h)	1.2–1.57	728	V	523 K	77, 0.04	2.0	[10]
HiPco (purified)	0.9–1.3	1300	V	393 K/1 Pa	303, 3.1	0.25	[23]
HiPco (purified)	0.9–1.3	1300	V	393 K/1 Pa	77, 0.1	1.8	[23]
HiPco	–	720	V	–	77, 5	2.0	[24]
					296, 9	0.6	[24]
HiPco		937	–	–	303, 10	0.3	[25]
PANI-MWNT	–	–	PCT	–	398, 6	0.5	[26]
MD-CNT	–	170, 258	Electrochemical	–	<293, <0.1	0.35	[14]

with carbon-hydrogen interaction and predict adsorption rates in optimized materials up to 2 wt.% at 70 MPa and 293 K [1,2,5,6]. Hydrogen adsorption in porous solids has been studied first for high surface area activated carbons. Nevertheless, it was found that only a small fraction of the pores in the wide pore-size distribution are effective for hydrogen storage [7,8]. Recent discovery of single wall carbon nanotubes has generated renewed interest in the use of porous nano-carbon materials for hydrogen storage. Indeed, the very narrow cylindrical pores combined with the surface high aromatisation, make nanomaterials potential candidates for hydrogen storage media [9–11].

From these works it has been demonstrated that the morphology and microstructure of carbon nanotubes, parameters controlled during the synthesis process, significantly affect their hydrogen storage capability [12,13]. The goal is to synthesis porous nanocarbons with large specific surface area per unit volume. Thus, novel carbon nanotube preparation methods are under investigation. Carbon nanotube synthesis by metal dusting process [14], carbon nanomaterial synthesis by using oil seeds and fibrous plant [15] and polymeric precursors [16] are novel methods already developed. Moreover the surface modification of the carbon materials by adding and dispersing reactive groups like metals [17] or by obtaining M

(metal)–C composites [18] in order to improve hydrogen adsorption capacity of materials are studied.

From Tables 1 and 2, it can be concluded that no general trend is observed for the experimental data corresponding to carbon nanotubes [4,10,14,19–27] and carbon nanofibers [11,24,25,27,28]. Material purification which has an important effect on the microporosity development of the material seems to increase gas adsorption sample capacity. As it has been analyzed in the literature [25,29–36], the high results dispersion and low reproducibility of experimental measurements in carbon nanotubes are mostly consequences of experimental errors such as non-purified samples, use of low purity hydrogen, sonication bar material and so on. In addition, each of the three existing methods used to estimate the hydrogen storage capacity of adsorbents (volumetric, gravimetric and temperature programmed desorption (TPD)) has its shortcoming.

The activated carbons are also widely studied in the literature as presented in Table 3 [1,9,15,27,33,35–42]. It has been demonstrated that narrow pores have maximum effects on gas storage efficiency while mesoporosity add to the total pore volume but is unfavorable for volumetric adsorption capacity. The gravimetric hydrogen storage capacities obtained by different authors are quite concordant in particular for

Table 2 – Hydrogen storage capacities in GNF at different conditions collected from literature.

GNF	Type	Set-up	Degassing conditions	T(K), P(MPa)	wt.%	References
CVD	herringbone	V	1173 K	300, 16	0.22	[27]
				77, 0.45	0.17	
CVD, purif. HCl	Platelet, D = 200–500 nm	G	473 K	303, 0.1	0.34	[28]
GNF		V	–	296, 9	0.3	[24]
GNF		V	656 K	303. 10	0,2	[25]
CVD brut	herringbone	V	673 K	293, 17	0.22	[11]
Purif. HCl	D = 20–500 nm		vacuum		0.34	
Purif. HNO3					0.28	

Table 3 – Hydrogen storage capacities in chemically activated carbons at different conditions collected from literature.

Material	SBET (m²/g)	Set-up	T(K), P(MPa)	wt.%	References
AX21	2575	GV	293, 70	1.6	[1]
AX21	2800	V	77, 50	5.2	[34]
AX21	2800	V	77, 3.5	5.5	[33]
AX21	2800	V	273, 5	0.5	[33]
AX21	3000	V	298, 6	0.5	[38]
AC	–	V	77, 0.1	4.5	[40]
Saran	1600	V	298, 16	0.42	[27]
Activated coal	1675	V	298, 10	0.6	[35]
Norit	1350	G	298, 12.5	0.75	[36]
Norit GSX	933	V	77, 0.1	1.53	[37]
Picactif SC	–	V	290, 12	1.0	[9]
CM5A-8	1646	V	77, 6	2.7	[39]
CM5B-9	946	V	77, 6	2.6	[40]
Carbon from soyabean	41	–	293, 1.1	1.09	[15]
Carbon from baggas	187.66	–	293, 1.1	0.66	[15]
Ni-AC-N	107	V	293, 3	0,53	[41]
AC	2560	V	77, 0.7	4.5	[41]

commercially available activated carbons at very high pressure up to 70 MPa and different temperatures from 293 K to 77 K [1,5,33,34].

From the analysis of Tables 1–3 the maximal hydrogen adsorptions are obtained at low temperatures and hydrogen adsorption capacity increases with pressure. The highest values of hydrogen adsorption gravimetric and volumetric storage are reported for a commercial activated carbon by Weinberger and Darkrim Lamari on a very high pressure device at 50 MPa and 77 K equal to 5 wt.% and 54 kg m^{-3} respectively [34]. Different types of materials exhibiting various porosities have been investigated. They obtained from a practical point of view that the maximal packing density is a relevant parameter that permit to maximize the volumetric hydrogen storage as demonstrated earlier. At room temperature, the maximum hydrogen storage capacity at high pressure 70 MPa reported in the literature is about 2 wt.% [1]. Meanwhile, others publications have reported hydrogen storage at high pressure using the same device than previously for reproducible purpose on various activated materials [43]. Further systematic studies on surface functional groups, pore and surface microstructure, thermodynamic and kinetic properties of pure and modified carbon nanomaterials are needed to understand and interpret the hydrogen adsorption on carbon nanomaterials [30,31,44–47]. To summarize, the real mechanism of hydrogen adsorption in different porous carbon materials having different microstructures is still to be clarified, however the simulations propose that the hydrogen molecules are adsorbed at different reactive sites on the solid material following different mechanism of adsorption.

Based on the literature review of the last decade, the present work provides reliable interpretation of hydrogen adsorption equilibrium measured accurately at room temperature and high pressures up to 70 MPa for three typical carbon material

varieties (GNF, SWNT and AC) and discussed with the help of different surfaces and pore analysis methods.

2.　Experimental method

The porous carbons used in this work are (i) GNF synthesized by CVD method [11], (ii) SWNT obtained by arc discharge method [13] and (iii) Commercial activated carbons with specific porosity (AC35, AC32) from CECA (France). The catalytic chemical vapor deposition (CVD) is a promising process concerning the large scale production of different kinds of carbon nanostructures [48,49]. The catalyst material, deposition temperature and the used hydrocarbon are the main parameters responsible for the formation of a desired structure. By optimizing these parameters, nanofibres with herringbone structure were synthesized. Mixing the hydrocarbon with H$_2$ at different rates leads to herringbone nanofibers with different angles of attach of graphene sheets to the central canal of the fiber were deposited. In all cases the material was refined and enriched by additional wet-chemical post-treatments.

Nanofibres were prepared from CO disproportionate over a MgO supported Co catalyst. Catalyst preparation: Citric acid (Riedel-de Haën), cobalt nitrate (Normapur Prolabo) and magnesium nitrate (Prolabo) are dissolved in 20 ml water. After dissolution, the aqueous solution was boiled under air and the nitrates are reduced by citric acid. A solid was obtained.

The above-described product was placed in a cylindrical silica reactor in a furnace. The catalyst, reduced by H$_2$ for 7 h at 873 K was reacted during 4 h at 785 K with a CO + H$_2$ mixture with 10%, 16% and 26% H$_2$ over 0.2 g of the catalyst. The "raw nanofibres" were obtained. The X-Ray analysis (Fig. 1) of the three raw samples synthesized with different H$_2$ ratio does not show any structural difference between these three samples. Then we have chosen one of the raw nanofibres, the sample synthesized with 16% of H$_2$, for the purification process. The chosen "raw product" was heated until ebullition by a high excess of concentrated hydrochloric acid. Then the deposit was washed with distilled water until the absence of chloride precipitate by addition of aqueous silver nitrate. The carbon content of the "purified nanofibre" was calculated as 98.5%.

Fig. 1 presents the X ray diffraction pattern of the raw samples synthesized with different rates of H$_2$ (10, 16, 26%) and the high resolution TEM image of the purified GNF sample. The TEM image shows no alteration of plans of graphite by acid treatment. The fiber is of herringbone type with 40 nm of diameter and 10 nm of internal diameter. The diffraction pattern shows that the materials have present the same nanometric structure, characteristic of the carbon arrangement constituted by separated plans by a distance varying between 0,3 nm and 0,52 nm. We cannot observe a noticeable difference between materials synthesized with different rates of hydrogen flow. We can observe on diffraction pattern the Co peak which is used as catalyst during the synthesis process. The difference between the intensity of Co peak on the three diffractograms is due to the amount of Co used for each synthesis.

SWNTs were obtained by arc discharge method by using the bi-metallic catalysts nickel and yttrium with the molar ratio of
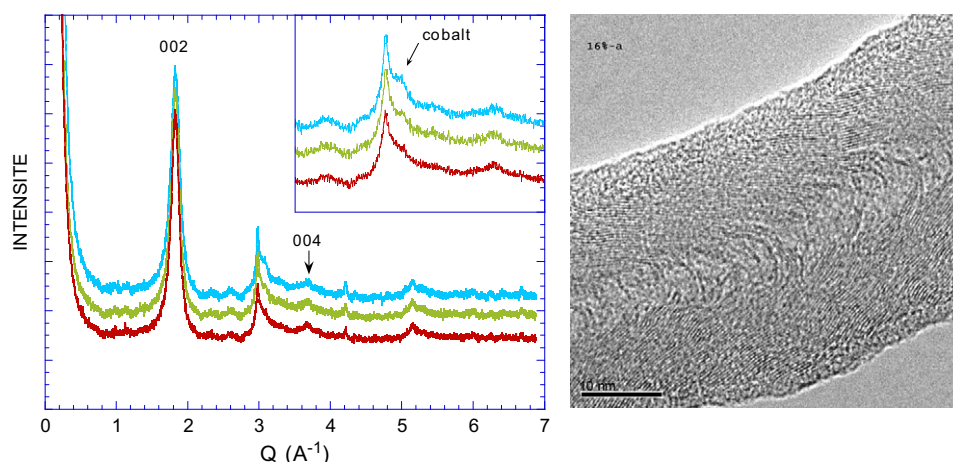
Fig. 1 – Left: X ray diffraction pattern (blue: 10% H₂, green: 16% H₂, red: 26% H₂,). Right: high resolution TEM characterization of the purified fiber (16% H₂).

(C/Ni/Y 94.8: 4.2: 1). The sample is purified by HCl treatment and by thermal oxidation at up to 700 K. During the thermal oxidation about 30% of the material is burned off, mainly corresponding to CO and CO_2 production. The Fig. 2 shows the Raman spectra (l = 514.5 nm, T = 298 K) of the material in RBM mode (70–180 cm^{-1}) and at high frequencies of the raw, thermal oxidized and acid purified SWNT. The analysis of spectrum distinguishes two frequency regions. In the high frequency region, between 1500 and 1600 cm^{-1}, the peaks considered as a signature of the existence of single walled tubes in a sample are localized. The Raman peak is centered at 1550 cm^{-1} which is assigned to the E_{2g} stretching mode in graphite [50]. The intermediate frequency region gives information on the chirality of the nanotubes. The peak at 1350 cm^{-1} which appeared in the Raman spectra of the purified sample, is induced by disorder or crystallographic defects which are located in the nanotube walls and ends. The peaks associated to the stretching modes are visible at about 1550 cm^{-1}.

Physical adsorption is mainly attributed to Van der Waals forces and electrostatic forces between adsorbate molecules and the carbon atoms which composed the main part of the adsorbent surface. Thus, adsorbents are characterized in terms of their surface properties such as the specific surface area. A large surface area is preferable for providing large adsorption capacity, but the creation of a large internal surface area in a limited volume inevitably gives rise to large numbers of small sized pores between adsorption surfaces. The size of the micropores determines the accessibility of adsorbate molecules to the internal adsorption surface, therefore the pore size distribution of micropores is another important property for adsorption process.

The activated carbons and activated carbon fibers are essentially microporous materials with a negligible contribution of meso- and macroporosity. Porous texture characterization of all the samples was performed by physical adsorption of N_2 at 77 K using Coulter apparatus. The micropore volume was determined by application of Dubinin–Radushkevich equation to the N_2 adsorption isotherm at 77 K up to P/P0 ≤ 0.1 [51]. One of the advantages of N_2 adsorption is

that it covers relative pressures from 10^{-8} to 1, which results in adsorption in the whole range of porosity. When N_2 adsorption at 77 K is used for the characterization of microporous solids, diffusional problems of the molecules inside the narrow porosity range can occur. To overcome this problem, the use of other adsorptives has been proposed in the literature [43]. CO_2 adsorption either at 273 K or 298 K is an easy alternative to N_2 adsorption for the assessment of the narrow microporosity [9]. The higher adsorption temperature
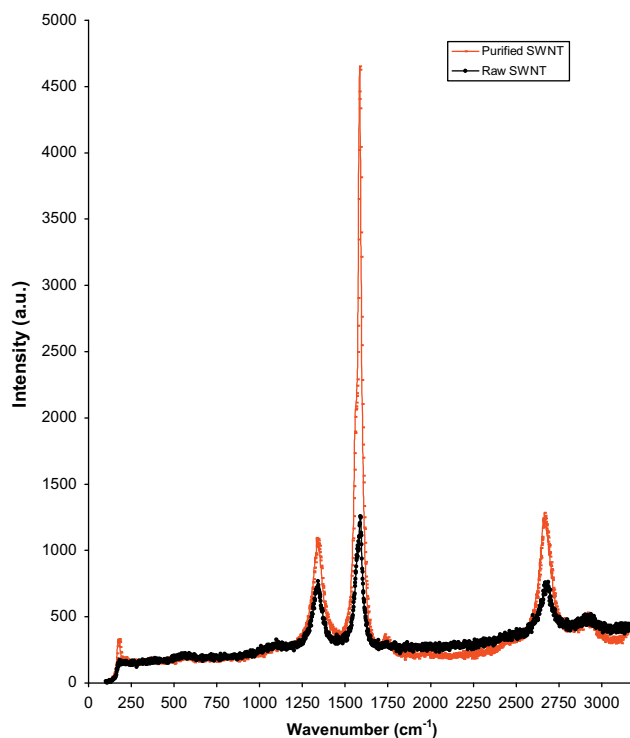

Fig. 2 – Raman spectroscopy at low and high frequencies of the raw (black), purified by acid treatment and by thermal oxidation (red) SWNT (λ = 514.7 nm). Intensity in arbitrary units is plotted versus the Raman shift in cm^{-1}.

used for CO_2 adsorption compared to N_2 adsorption at low temperature, results in a larger kinetic energy of the molecules allowing them to enter into narrow pores.

The Table 4 summarizes the porous textures of the samples used, including the specific surface area and the microporous volume of the materials obtained from the adsorption of N_2 at 77 K. These materials cover a wide range of micropore size. One can noticed that the specific surface areas of the raw nanocarbons were less than the value (150 $m^2 g^{-1}$) reported on the second column of the Table 4. The opening of the SWNTs by thermal treatment and creation of defects on fiber walls by hard acid treatment have been proposed as explanation for the micropore development [22,52]. The defects on the C surface of the nanomaterials could be deduced from the peak situated at 1350 cm^{-1} of the Raman spectra (Fig. 2). In the present study only the purified nanocarbons have been used for investigating gas adsorption capacity. The porous texture of the different materials of the present study shows that all the samples have a high micropore volume. The activated carbons microporosity and pore volume are higher than those of nanocarbons.

3. Results and discussion

Despite the molecular interactions between hydrogen gas and carbon adsorbent solid surface are weak, they are numerous [2,3,5,6,53–56]. Thus this point implies difficulties for accurate adsorption measurements and has probably leaded to disperse and erroneous storage values in the literature. Consequently, we chose an experimental procedure which enables both leak detection and negligible systematic errors. Thus, in the present work, we used an adapted experimental device which was designed and built for adsorption investigation of low solid-gas interaction systems. A well calibrated and high precision volumetric-gravimetric apparatus (0.52% accuracy) for adsorption measurements of gas phase hydrogen in carbonaceous materials devoted to hydrogen storage investigation, has been designed, built and used [57]. The performance of the apparatus was assessed by helium and hydrogen adsorption in several porous materials [34]. The adsorption equilibrium was realized at 5 MPa and at room temperature. Comparison to results obtained up to 70 MPa on the previously developed very High Pressure Device (HPD-RT) already published in the literature for different material investigation [1,11,22,43] is also

given. Previous to the adsorption isotherm measurements, the sample was degassed at 523 K during 24 h under vacuum and its helium density was measured at high temperature and low pressure following the process described in the literature [22,34,57]. Porous material real density is crucial for the adsorption property study. The calculation of the amount of gas adsorbed on a solid surface requires the correct definition of the gas-solid limit i.e. Gibbs dividing surface, delimiting the volume accessible to the gas. The use of Helium gas is due to, on the one hand, its small atom diameter that enables to penetrate into the small submicropores, and on the other hand, its low interactions with the solid surface. Thus, the excess of adsorption were calculated by taking in account the dead volume from the skeleton density, determined at 700 K to avoid helium adsorption, of the materials which are about 1.9 $g\,cm^{-3}$ instead of the crystal graphite density equal to 2.2 $g\,cm^{-3}$.

Table 5 groups the excess adsorption results for hydrogen at 293 K expressed in mmol/g corresponding to the samples of the present study. The last column corresponds to very high pressure measurements obtained on the very HPD-RT up to 700 bars. The maximal values for AC35 (1 wt.%) and Tubes/Fibre (0,2–0.3 wt.%) have been obtained at 70 MPa. It can be seen that, nanotubes and nanofibers present the lowest hydrogen adsorption capacities at room temperature, according to their low porosity development in particular their low specific area development and thus the number of adsorption sites which then reduce the possible gas-solid interaction. The difference between the amounts adsorbed on both samples may be due to the difference of active surface and developed microporous volume. Annealing the samples at high temperature in inert atmosphere may increase the porosity and surface area by the removal of blocking functional groups at the entry ports of SWNTs and the defects on the external wall of the nanofibres. The hydrogen adsorption isotherms obtained for the rest of the materials seem to indicate that the higher the porosity development of the sample, the higher the adsorption site number, the higher the hydrogen adsorption capacity. These results are compatible with published results for identical materials [31,44–47]. We can observe from the Tables 4 and 5 that hydrogen adsorption capacity at high pressure of the materials increases with total micropore volume from 0.28 $cm^3 g^{-1}$ (GNF sample) up to 0.54 $cm^3 g^{-1}$ (AC35 sample). At higher micropore volume values the sample with the highest porosity development presents the highest hydrogen adsorption capacity. Also,

Table 4 – Porous texture obtained from nitrogen adsorption isotherms at 77 K: specific area (column 2) and total micropore volume (column 3) for the carbon materials studied in the present work.

Sample	SBET $m^2.g^{-1}$	Total micropore Volume $cm^3.g^{-1}$
SWNT (purified)	195	0.32
GNF (purified)	230	0.28
AC32	1740	0.42
AC35	1200	0.54

Table 5 – Excess Hydrogen adsorption equilibrium in mmol g^{-1} at 293 K and various gas pressures for the carbon materials investigated in the present study.

Material	Hydrogen excess of adsorption in mmol.g^{-1}				
	$p = 5$ bar	$p = 10$ bar	$p = 20$ bar	$p = 50$ bar	$p = 700$ bar
SWNT	0.03	0.07	0.13	0.30	–
GNF	0.02	0.05	0.09	0.33	1.13
AC32	0.13	0.24	0.45	0.97	–
AC35	0.29	0.34	0.68	1.42	4.62

on one hand, there seems to be no correlation between the specific area and hydrogen adsorption capacity on activated carbons measured even at lower pressure and room temperature since the AC32 sample which exhibits the highest specific surface area equal to $1740 \, m^2 \, g^{-1}$ adsorbs less hydrogen than the AC35 sample with a lower specific surface area equal to $1200 \, m^2 \, g^{-1}$. On the other hand, since the micropore volume is more favourable to adsorption in AC35 sample than AC32 sample, it seems to be in direct correlation with the amount of gas adsorbed in the AC35 material. It was suggested then that the amount of hydrogen adsorbed on carbon surface should be enhanced by improvement of the sample micro-structure and the gas thermodynamic conditions [2,3,5,6,53,54]. Experimental results demonstrated that the volumetric-gravimetric apparatus and the uptake data processing method can provide an accurate adsorption measurement for gas phase hydrogen in porous carbon materials.

In comparison with simulation data, our results demonstrate clearly that the main classes of porous carbon materials (GNF, SWNT and AC) with moderate specific areas (less than $1000 \, m^2 \, g^{-1}$) and microporous volumes ranged from 0.3 to $0.5 \, cm^3 \, g^{-1}$ exhibit comparable adsorption capacities due to the local physisorption phenomenon because of van der Waals hydrogen-carbon interaction (although complex chemical processes could occur with small contribution).

The surface adsorption of hydrogen on carbon walls contributes to the free space hydrogen adsorption. We measured the contribution of free space hydrogen adsorption in the material porosity and the surface adsorption on our experimental set up. Thus, considering the adsorption amounts, the specific surface area and the total micropore volume, we can observe that the available free volume for adsorption process is mainly located on the material surfaces due to the low physical gas-solid interaction range. At room temperature, this latter is of the order of the gas molecule diameter [1,2]. One noticed that the higher the specific area and microporous volume (optimization of material porosity) the higher the gas adsorption. At high pressure and room temperature (the present work) or moderate pressure and low temperature (our previous work [34]), the contribution of the specific area/microporous volume to gas adsorption is maximal due to gas-solid interaction range. Thus, we calculated for AC35 material at both 293.15 K and 77.4 K temperatures, the ratio of the gas adsorption with the specific area and the ratio of the gas adsorption with microporous volume. The values are in agreement with the ratio between the two temperatures ($\sim$3–4) leading for AC35 porous material to a linearity between the adsorption, specific area and micropore volume.

From a practical point of view, these adsorption amounts are not large enough for allowing an efficient storage of hydrogen gas at room temperature for a large range of pressure. Also, it is noticeable that further investigation of the thermal effects during high pressure charge and discharge in adsorbent packed bed for storage tanks is essential for hydrogen storage process optimization. The influence of the flow rate and storage pressure on the temperature could be then investigated [58,59]. In parallel, hydrogen adsorption–desorption cycling behaviour of GNF, SWNT and ACs have shown favourable charge-discharge kinetics at 77 K [9,34].

4.   Conclusion

Particular attention was focused on carbon sorption systems because they can store hydrogen with moderate size, weight and pressure. Concerning the storage of hydrogen in a hybrid tank system, the part adsorbed on a high performance adsorbent contributes to the reduction of operating pressure compared to high pressure compressed gas technology. Consequently, less weight for the storage system with better safety standards is feasible. This application is enhanced by improving graphitic nano-structure material properties. At room temperature, adsorption on the porous material, is gradually increasing with the porous volumes and specific areas of the different materials investigated. The enhancement of hydrogen adsorption might result from the increase of reachable local adsorption sites by material micropore development but also material bulk densities for volumetric storage optimization. The mechanism of hydrogen adsorption and desorption has to be clarified. For thus, the microstructure and the topology of the porous carbon materials considered for hydrogen adsorption has to be understood. That means qualifying and quantifying the functional groups by appropriate techniques, the thermodynamic and kinetic behaviour of pure materials as well as their surface modified and activated form. These improvements must be followed by technical advancements for developing and characterizing the adsorption sites in the carbon structure. These developments could facilitate the kinetic of charging and discharging hydrogen at room temperature and moderate-to-high pressure conditions. Further work could be done on the use of different materials (metals, ligands, functional groups, surface modification in order to increase the surface area and pore size) combined with carbon nanomaterials to enhance adsorbent-adsorbate interaction in order to use them as storage media for hydrogen gas. Formation of polymeric nanocomposites, electro less deposition of metals having huge interaction with hydrogen on nanotube surface, and metal deposit by using ligands like phosphazenes and phtalocyanines may be investigated as future works.

Acknowledgements

REFERENCES

[1] Darkrim F, Vermesse J, Malbrunot P, Levesque D. Monte Carlo simulations of nitrogen and hydrogen physisorption at high pressures and room temperature. Comparison with experiments. J Chem Phys 1999;110(8):4020–7.

[2] Darkrim F, Levesque D. Monte Carlo simulations of hydrogen adsorption in single-walled carbon nanotubes. J Chem Phys 1998;109(12):4981–4.

[3] Wang QY, Johnson JK. Molecular simulation of hydrogen adsorption in single-walled carbon nanotubes and idealized carbon slit pores. J Chem Phys 1999;110(1):577–86.

[4] Dillon AC, Jones KM, Bekkedahl TA, Kiang CH, Bethune DS, Heben MJ. Storage of hydrogen in single-walled carbon nanotubes. Nature 1997;386(6623):377–9.

[5] Darkrim F, Levesque D. Environmental application of surface reactivity analysis. Surf Interface Analysis 2002;34(1):97–9.

[6] Wang Q, Johnson JK. Optimization of carbon nanotube arrays for hydrogen adsorption. J Phys Chem B 1999;103(23): 4809–13.

[7] Gadiou R, Texier-Mandoki N, Piquero T, Saadallah S-E, Parmentier J, Patarin J, et al. The influence of microporosity on the hydrogen storage capacity of ordered mesoporous carbons. Adsorption 2005;11:823–7.

[8] Kowalczyk P, Solarz L, Do DD, Samborski A, Mac Elroy JMD. Nanoscale tubular vessels for storage of methane at ambient temperatures. Langmuir 2006;22(21):9035–40.

[9] Texier-Mandoki N, Dentzer J, Piquero T, Saadallah S, David P, Vix-Guterl C. Hydrogen storage in activated carbon materials: role of the nanoporous texture. Carbon 2004; 42(12–13):2744–7.

[10] Callejas MA, Anson A, Benito AM, Maser W, Fierro JLG, Sanjuan ML, et al. Enhanced hydrogen adsorption on single-wall carbon nanotubes by sample reduction. Mater Sci Eng B – Solid State Mater Adv Technol 2004;108(1–2):120–3.

[11] Kayiran SB, Darkrim Lamari F, Weinberger B, Gadelle P, Firlej L, Bernier P. Herringbone nanofiber synthesis by CVD method and hydrogen storage adsorption performance analysis. Int J Hydrogen Energy 2009;34:1965–70.

[12] Fazle Kibria AKM, Mo YH, Park KS, Nahm KS, Yun MH. Electrochemical hydrogen storage behaviors of CVD AD and LA grown carbon nanotubes in KOH medium. Int J Hydrogen Energy 2001;26:823–9.

[13] Bernier P, Maser W, Journet C, Loiseau A, Lamy de la Chapelle M, Lefrant S, et al. Carbon single wall nanotubes elaboration and properties. Carbon 1998;36(5–6):675–80.

[14] Chang JK, Tsai HY, Tsai WT. Effects of post treatments on microstructure and hydrogen storage performance of the carbon nanotubes prepared via a metal dusting process. Int J Hydrogen Energy 2008;182:317–22.

[15] Sharon M, Soga T, Afre R, Sathiyamoorthy D, Dasgupta K, Bhardwaj S, et al. Hydrogen storage by carbon materials synthesized from oil seeds and fibrous plantmaterials. Int J Hydrogen Energy 2007;32(17):4238–49.

[16] Kim BJ, Lee YS, Park SJ. Novel porous carbons synthesized from polymeric precursors for hydrogen storage. Int J Hydrogen Energy 2008;33(9):2254–9.

[17] Reddy ALM, Ramaprabhu S. Hydrogen storage properties of nanocrystalline Pt dispersed multi walled carbon nanotubes. Int J Hydrogen Energy 2007;32(16):3998–4004.

[18] Rud AD, Lakhnik AM, Ivanchenko VG, Uvarov VN, Shkola AA, Dekthyarenko VA, et al. Int J Hydrogen Energy 2008;33(4): 1310–6.

[19] Hirscher M, Becher M, Haluska M, Dettlaff-Weglikowska U, Quintel A, Duesberg GS, et al. Hydrogen storage in sonicated carbon materials. Appl Phys A 2001;72:129–32.

[20] Dillon AC, Heben MJ. Hydrogen storage using carbon adsorbents: past, present and future. Appl Phys A Mater Sci Process 2001;72(2):133–42.

[21] Kajiura H, Tsutsui S, Kadono K, Ata M, Murakami Y. Appl Phys Lett 2003;82:1105–7.

[22] Kayiran SB, Lamari Darkrim F, Levesque D. Adsorption properties and structural characterization of activated and nano-carbons. J Phys Chem B 2004;108(39):15211–5.

[23] Takagi H, Hatori H, Soneda Y, Yoshizawa N, Yamada Y. Adsorptive hydrogen storage in carbon and porous materials. Mater Sci Eng B – Solid State Mater Adv Technol 2004;108(1–2):143–7.

[24] Kojima Y, Kawai Y, Koiwai A, Suzuki N, Haga T, Hioki T, et al. Hydrogen adsorption and desorption by carbon materials. J Alloys Compd 2005;395:236.

[25] Xu WC, Takahashi K, Matsuo Y, Hattori Y, Kumagai M, Ishiya S, et al. Investigation of hydrogen storage capacity of various carbon materials. Int J Hydrogen Energy 2007;32:2504–12.

[26] Jurczyk MU, Kumar A, Srinivasan S, Stefanakos E. Polyaniline based nanocomposite materials for hydrogen storage. Int J Hydrogen Energy 2007;32:1010–5.

[27] Ahn CC, Ye Y, Ratnakumar BV, Witham C, Bowman RC, Fultz B. Hydrogen adsorption and cohesive energy of single-walled carbon nanotubes. Appl Phys Lett 1998;73(23):3378–80.

[28] Hanada N, Ichikawa T, Fujii H. Catalytic effect of nanoparticle 3d-transition metals on hydrogen storage properties in magnesium hydride MgH$_2$ prepared by mechanical milling. J Phys Chem B 2005;109(15):7188–94.

[29] Benard P, Chahine R. Storage of hydrogen by physisorption on carbon and nanostructured materials. Scripta Materialia 2007;56:803–8.

[30] Lamari Darkrim F, Malbrunot P, Tartaglia GP. Review of hydrogen storage by adsorption in carbon nanotubes. Int J Hydrogen Energy 2002;27(2):193–202.

[31] Bandosz Teresa J. In: Activated carbon surfaces in environmental remediation. 1st ed. Oxford: Elsevier; 2006.

[32] Luxembourg D, Flamant G, Beche E, Sans JL, Giral J, Goetz V. Hydrogen storage capacity at high pressure of raw and purified single wall carbon nanotubes produced with a solar reactor. Int J Hydrogen Energy 2007;32:1016–23.

[33] Poirier E, Chahine R, Bénard P, Cossement D, Lafi L, Mélancon E, et al. Storage of hydrogen on single-walled carbon nanotubes and other carbon structures. Appl Phys A Mater Sci Process 2004;78(7):961–7.

[34] Weinberger B, Darkim Lamari F. High pressure cryo-storage of hydrogen by adsorption at 77 K and up to 50 MPa. Int J Hydrogen Energy 2009;34(7):3058–64.

[35] Rzepka M, Lamo P, de la Casa Lillo MA. Physisorption of hydrogen on microporous carbon and carbon nanotubes. J Phys Chem B 1998;102(52):10894–8.

[36] Strobel R, Jorissen L, Schliermann T, Trapp V, Schutz W, Bohmhammel K. Hydrogen adsorption on carbon materials. J Power Sourc 1999;84(2):221–4.

[37] Schimmel HG, Nijkamp G, Kearley GJ, Rivera A, deJong KP, Mulder FM. Hydrogen adsorption in nanostructures compared. Mat Science Eng B 2004;108:124–9.

[38] Zhou L, Zhou YP, Sun Y. A comparative study of hydrogen adsorption on superactivated carbon versus carbon nanotubes. Int J Hydrogen Energy 2004;29(5):475–9.

[39] Terres E, Panella B, Hayashi T, Kim YA, Endo M, Dominguez JM, et al. Hydrogen storage in spherical nanoporous carbons. Chem Phys Lett 2005;403(4–6):363–6.

[40] Schimmel HG, Kearley GJ, Nijkamp MG, Visser CT, Jong KP, Mulder FM. Hydrogen adsorption in carbon nanostructures: comparison of nanotubes, fibers, and coals. Chem Eur J 2003; 9:4764–70.

[41] Zielinski M, Wojcieszak R, Monteverdi S, Mercy M, Bettahar MM. Hydrogen storage in nickel catalysts supported on activated carbon. Int J Hydrogen Energy 2007;32:1024–32.

[42] Hirscher M, Panella B. Nanostructures with high surface area for hydrogen storage. J Alloys Compd 2005;404–406:399–401.

[43] De la Casa Lillo MA, Lamari Darkrim F, Cazorla-Amors D, Linares- Solano A. Hydrogen storage in activated carbon fibers. J Phys Chem B 2002;106(42):10930–4.

[44] Zhou L. Progress and problems in hydrogen storage methods. Renew Sustain Energy Rev 2005;9:395–408.

[45] Satyapal S, Petrovic J, Read C, Thomas G, Ordaz G. The U.S. department of energy's national hydrogen storage project: progress towards meeting hydrogen powered vehicle requirements. Catalysis Today 2007; 120:246–56.

[46] Ross DK. Hydrogen storage: the major technological barrier to the development of hydrogen fuel cell cars. Vacuum 2006; 80:1084–9.

[47] David E. An overview of advanced materials for hydrogen storage. J Mat Processing Technology 2005;162(173): 169–77.

[48] Browning DJ, Gerrard ML, Lakeman JB, Mellor IM, Mortimer RJ, Turpin MC. Studies into the storage of hydrogen in carbon nanofibers: proposal of a possible reaction mechanism. Nano Lett 2002;2(3):201–5.

[49] Xu W, Tao Z, Chen J. Progress of research on hydrogen storage. Progr Chem 2006;18(2–3):200–10.

[50] Lafi L, Cossement D, Chahine R. Raman spectroscopy and nitrogen vapour adsorption for the study of structural changes during purification of single-wall carbon nanotubes. Carbon 2005;43(7):1347–57.

[51] Dubinin MM. In: Walker Jr PL, editor. Chemistry and physics of carbon, vol. 2. New York: Marcel Dekker; 1996.

[52] Züttel A, Sudan P, Mauron Ph, Kiyabayashi T, Emmenegger Ch, Schlapbach L. Hydrogen storage in carbon nanostructures. Int J Hydrogen Energy 2002;27:203.

[53] Darkrim-Lamari F, Weinberger B, Kunowsky M, Levesque D. Material design by molecular modelling of hydrogen storage. AIChE J 2009;55(2):538–47.

[54] Darkrim F, Aoufi A, Levesque D. Quantum contribution to gas adsorption in carbon nanotubes. Mol Sim 2000;24(1–3):51–61.

[55] Weinberger B, Darkrim Lamari F, Beyaz S, Gicquel A, Levesque D. Molecular modelling of H_2 purification on Na-LSX zeolite and experimental validation. AIChE J 2005;51(1):142–8.

[56] Weinberger B, Darkrim Lamari F, Levesque D. CO2 capillary condensation and adsorption of binary mixture. J Chem Phys 2006;124:234712.

[57] Weinberger FD, Lamari A, Veziroglu S, Kayiran SB, Beauverger M. New accurate gravimetric volumetric adsorption method for low gas-zeolite interaction systems. Int J Hydrogen Energy 2009;34:3191–6.

[58] Lamari M, Aoufi A, Malbrunot P. Thermal effects in dynamic storage of hydrogen by adsorption. AIChE J 2000;46(3):632–46.

[59] Levesque D, Darkrim Lamari F. Pore geometry and isosteric heat: an analysis of carbon dioxide adsorption on activated carbon. Mol Phys 2009;107(3–4):1–7.